Materials Today Communications 50 (2026) 114556

Contents lists available at ScienceDirect

Materials Today Communications

journal homepage: www.elsevier.com/locate/mtcomm

Dissolution kinetics of poly(styrene-co-acrylonitrile) below and above its glass transition temperature

Sandra Litwin [a], Giuseppe Melilli [a], Luc Vincent [a], Mark C.P. Roelands [b], Ruud Cuypers [b], Pieter Janssen [c], Andreia.F. Sousa [d], Nicolas Sbirrazzuoli [a,*], Nathanael Guigo [a,e,**]

[a] Institut de Chimie de Nice, Université Côte d'Azur, CNRS, UMR 7272, Nice 06108, France
[b] TNO, Kesslerpark 1, Rijswijk 2288 GS, the Netherlands
[c] Trinseo Netherlands B.V., Innovatieweg14, Hoek, 4542 NH, the Netherlands
[d] CICECO-Aveiro Institute of Materials, Department of Chemistry, University of Aveiro, Portugal
[e] Mines Paris, PSL University, Center for Material Forming CEMEF (UMR CNRS 7635), 06904 Sophia Antipolis Cedex, France

ARTICLE INFO

Keywords:
Polymer dissolution
Physical recycling
Glass Transition

ABSTRACT

The dissolution behaviour of poly(styrene-co-acrylonitrile) (SAN) was examined across a broad temperature range to identify the governing thermodynamic and kinetic factors. Two high-boiling solvents with contrasting affinities for SAN, namely diethyl succinate (DS, RED = 0.69) and triethyl citrate (TC, RED = 1.37), were selected to study dissolution below and above the SAN glass transition temperature ($T_g \approx 105$ °C). Isothermal mixing calorimetry (30–150 °C) showed complete SAN dissolution in DS above 45 °C, with exothermic dissolution enthalpies decreasing from 20 J g^{-1} at 45 °C to 6 J g^{-1} at 120 °C, the latter reflecting polymer–solvent interactions once the glassy-rubbery transition no longer contributes. In TC, SAN did not dissolve at 30 °C and was only partially dissolved up to 80 °C; complete dissolution occurred only above T_g, with an enthalpy of ~6 J g^{-1} at 120 °C. ATR-FTIR monitoring revealed strong effects of solvent quality and temperature on induction time. SAN chains appeared in solution after 480 s in DS but after ~5000 s in TC at 45 °C, evidencing significant segmental-relaxation limitation in TC. Above T_g, induction times sharply decreased to 120 s in DS and 360 s in TC at 120 °C. Isoconversional kinetic analysis showed that dissolution in DS above T_g is diffusion-controlled, with low activation energies (6–15 kJ mol^{-1}). Below T_g, SAN dissolution transitions from segmental-relaxation-controlled (increasing to 41 kJ mol^{-1}) to diffusion-controlled at higher conversion. Dissolution in TC below T_g exhibited even stronger relaxation control, with E_a reaching 116 kJ mol^{-1} .

1. Introduction

Acrylonitrile-butadiene-styrene (ABS) is widely used in household applications, electrical and electronic equipment, toys, and automotive industry amongst others. It is considered the most used engineering plastic [1]. Therefore, developing an effective recycling strategy for this material is of significant importance. ABS is made of a poly (styrene-co-acrylonitrile) (SAN) matrix which contains dispersed polybutadiene-based rubber particles (PBR).

Various studies [2–4] investigated how ABS behaves during mechanical recycling particularly when the material is subjected to re-extrusion cycles. It was noticed post-reprocessing colour change [2], impact [3] and fracture [4] resistance properties losses. The decrease in mechanical performances was attributed to chain scissions in SAN and PBR crosslinking under reprocessing.

Indeed, mechanical recycling is a simple, cheap, and very low energy intensive recycling method. In mechanical recycling, plastic parts are shredded, sometimes then recompounded with new polymers or additives, and new products are made. Due to the accumulation of contaminations and degradation of the polymers and additives, in most cases, mechanical recycling leads to down-cycling: the demands placed upon the new product are less challenging than the ones on the waste source. Mechanical recycling has been around for a while, but the technology has limits. One needs access to high-purity waste streams, and it's not a true infinite loop recycling technique due to the down-cycling in each step [1].

* Corresponding author.
** Corresponding author at: Institut de Chimie de Nice, Université Côte d'Azur, CNRS, UMR 7272, Nice 06108, France.
E-mail addresses: Nicolas.Sbirrazzuoli@univ-cotedazur.fr (N. Sbirrazzuoli), Nathanael.Guigo@univ-cotedazur.fr (N. Guigo).

https://doi.org/10.1016/j.mtcomm.2025.114556
Received 24 October 2025; Received in revised form 5 December 2025; Accepted 22 December 2025
Available online 23 December 2025

In chemical recycling on another hand, plastic waste is reduced to basic chemicals, such as monomers or pyrolysis oil [1]. This is often a very energy intensive process, sometimes even more energy intensive than the production of virgin polymers [5]. However, a wide variety of plastic waste can be accepted [6].

In physical recycling, the plastic waste is dissolved in a solvent [7,8]. In particular, the physical recycling of a plastic material via the dissolution-precipitation technique enables the recovery of polymers with virgin-like competitive properties [9]. This also enables the isolation and purification of the polymer matrix from the unwanted additives or contaminants and allows the re-use of some additives [10]. These non-polymeric components can be removed via various filtration techniques [11], the solvent is then evaporated, and the pure polymer remains [7,8]. The advantages are that the filtration can be very selective, the polymer should not suffer degradation unless it undergoes heating [8], and the polymer chains remain intact, all while keeping the energy footprint limited [1]. Physical recycling is a relatively new technique but has garnered a lot of interest recently [12]. The low energy intensity, combined with the wide variety of waste it can accept [7], makes it a very promising technology [8].

Physical recycling is therefore suitable for the recycling of highly formulated plastics such as ABS. At the moment, there are several commercial companies working at or towards kiloton scale. Well-known successful physical recycling was performed by CreaSolv®SB process [13] (CreaCycle Gmbh company) for the separation of ABS and high impact polystyrene (HIPS) from unwanted non-dissolved components, contaminants and brominated flame-retardants [14]. Polystyrene packaging waste were recycled and recovered free of additives through UpSolv's process (ex Polystyvert), using of cymene as a solvent and an anti-solvent [15–17]. PureCycle [18] elaborated a dissolution-precipitation technology which enabled the recovery of virgin-like recycled polypropylene from post-consumer and post-industrial polypropylene waste. The dissolution was performed in supercritical butane, contaminants such as pigments, fillers, dirt and polymers were separated out, and the recycled polymer was recovered through precipitation via decompression. The recycled polypropylene can be used for packaging applications. Trinseo developed the dissolution-based recycling of post-consumer polystyrene [19,20], which was recovered free of impurities such as other polymers, dust and metal after filtration. This technology enabled the commercialisation of a food-grade polystyrene containing 30 % of recycled polystyrene and a 18 % decrease in the carbon footprint of the material compared to the virgin counterpart. Trinseo also developed a dissolution technology for the recycling of polycarbonate from mixed (with plastics, metal or glass) end-of-life materials [21,22]. The polycarbonate was dissolved in the solvent, whereas the non-polycarbonate fractions were filtered out and can be re-engaged in further recycling processes. The recycled polycarbonate can be re-compounded and a significant reduction in the carbon footprint of the recycled polycarbonate was observed compared to the virgin's one.

To this day, there are few studies on the physical recycling of ABS [23]. A recent one [24] reports the successful recovery of ABS from toy waste and the probable elimination of antioxidants, heat stabilizers, plasticizers and fluoro-compounds using an acetone/water solvent system for the dissolution-precipitation process. The loss of additives led to a slight drop in thermo-mechanical properties as the recovered SAN-rich phase material was not re-formulated after recycling. Another study [25] aimed at investigating the mechanical properties of a post-consumer ABS which underwent several dissolution/recovering cycles in acetone, sometimes followed by reprocessing. Even though the purpose was not to remove additives, some of them inevitably dissolved in the solvent, which induced the degradation of the recovered ABS, causing a decrease in the thermo-mechanical properties. Both SAN matrix and PBR were affected under reprocessing. Post-production ABS was dissolved in acetone and CreaSolv®SB solvent formulation and then filtered or centrifuged in order to eliminate inorganic pigments [11]. The removal ratio was above 80 % except for centrifuged CreaSolv®SB solutions. In another investigation, a phosphate flame-retardant was successfully removed from a PC/ABS resin [26] employing N, N-dimethylcyclohexylamine (DMCHA) as a solvent. This process enabled the recovery of the components with a high degree of purity.

Thus far, the process of polymer dissolution has been characterized and monitored with the help of techniques such as FTIR imaging [27]; optical microscopy and differential refractometry [28], interferometry [29,30], ellipsometry [31], steady-state fluorescence [32] and nuclear magnetic resonance (NMR) [33]. These techniques allow the investigation of swelling and dissolution mechanisms and rates. However, the *in-situ* monitoring of ABS and or SAN dissolution has not been extensively investigated. Only one previous work in our team [34] demonstrated that correlating data from calorimetry and FTIR experiments enabled to identify the thermodynamic and kinetic determining steps during SAN dissolution. From a thermodynamic standpoint, the dissolution of SAN is governed by the glassy to rubbery transition before having the proper chain dissolution. This is associated with an increase of the activation energy at the end of the process. However, the methyl-ethyl-ketone (MEK) is a low-boiling point solvent, thus limiting the temperature range for dissolution.

The novelty of this research is that a special emphasis is made on the temperature dependence of the dissolution process of SAN on a particularly large temperature domain (~120 °C), i.e. spanning from 30 °C to 150 °C. This is much larger compared to previous investigations that usually employ either a single temperature (ambient temperature, Lu et al. [24]) or a very narrow temperature range (25 °C to 40 °C for Arostegui et al. [25] or from 30 to 60 °C for Melilli et al. [34]). It is particularly important to determine how this dependence is affected by positioning the dissolution process below or above the glass transition temperature of SAN (T_g ~ 105 °C). Therefore, we have used in this paper, solvents with a relatively high boiling point to monitor the dissolution process for temperatures above the glass transition of SAN. Thus, the comparison of the SAN dissolution in a large temperature domain would allow to determine the difference in dissolution dynamics especially below and above the glass transition of SAN. For this purpose, high boiling point solvents, relative to the glass transition temperature of SAN, should be employed. For practical application and relevance in a dissolution process, the boiling point should also not be too high, as the solvent will need to be evaporated at some point. Moreover, the likeliness of the solvent - i.e., good or less good solvent (from the perspective of the Hansen solubility parameter) towards SAN dissolution – is impacted by the temperature at which the dissolution occurs. This study aims to understand these aspects which are important in the perspective of having tuned conditions for SAN dissolution. This will pave the way for optimizing conditions for ABS physical recycling. Two different solvents namely diethyl succinate (DS) and triethyl citrate (TC) were employed to monitor *in situ* the SAN dissolution with mixing calorimetry and FTIR spectroscopy. These solvents were chosen for their distinct positions within (good solvent) and outside (poor solvent) the SAN's Hansen sphere. This should allow to take the description and comprehension of the thermodynamic and kinetic determining steps of SAN dissolution one step further.

2. Materials

SAN pellets (poly(styrene-co-acrylonitrile), M_w = 90000 g/mol, 3.8 × 2.7 × 2.1 mm) and pieces (10 ×7.5 ×4.08 mm and 10 ×7.5 ×1.36 mm) were supplied by Trinseo NL. Diethyl succinate (purity ≥ 99 %) and triethyl citrate (purity ≥ 99 %) were purchased from Sigma-Aldrich and used as received.

3. Methods

3.1. Reaction calorimetry

The calorimetric monitoring of SAN dissolution in both the solvents (ratio 20 %w/v SAN in solvent) was performed in a Setaram C80 Calvet calorimeter whose temperature and heat flow calibrations were performed with indium and wood alloy standards. After placing polymer pellets or pieces (one piece of 4.08 mm thickness or three pieces of 1.36 mm thickness) in the bottom mixing cell, solvent was poured in the top cell, the two of them being separated by a Teflon membrane. The whole system is hermetic and placed in the calorimeter. A reference cell is empty because no matter the solvent nor the temperature (even the high ones), no solvent effect was observed. Before launching an experiment, equilibration of the apparatus at the setting temperature was made until stabilization of the baseline. A metal rod with a pointy end was used to perforate the membrane. Isothermal SAN dissolution experiments were performed in different solvents at several temperatures for a duration of 15 h. The heat flow measurement started one minute before perforating the membrane to ensure that the whole phenomenon was recorded. The heat flow (mW) was recorded as a function of time and was normalized to the sample mass. The overall enthalpy of dissolution ΔH_{diss} (J/g) was calculated after integration of the heat flow curves using a horizontal right baseline on the STARe software. The precision on the enthalpies is of ±1 % according to Setaram's specification, and variability observed on replicates are in the same range. The extent of conversion α^{CAL} was calculated as follows:

$$\alpha^{CAL}(t) = \Delta H(t) / \Delta H_{tot} \quad (1)$$

3.2. Fourier-transformed infrared spectroscopy

The dissolution monitoring (concentration 20 %w/v SAN in solvent) was carried out on a Thermo Scientific Nicolet iS20 spectrometer equipped with a PIKE Gladi ATR component and a heating plate controlled by a PIKE Temperature Controller. Measurements and air background were recorded with a 4 cm^{-1} resolution and 64 scans. The dissolution was followed isothermally during 10 h for temperatures set between 30 °C and 120 °C, with a spectrum recorded every 2 min. First, the air background was recorded, then the solvent was injected after a 2-minute time-lapse.

The system used to monitor the dissolution by FTIR is presented Fig. 1. The SAN pellets were placed around the crystal so that bands associated with SAN are not detected before the proper dissolution starts. The system is hermetically sealed with a Teflon cylinder, a device allowing the solvent injection and pressure is applied through the ATR screw and tip.

The extent of conversion, α^{FTIR}, was then calculated based on the band related to the aromatic C-H out-of-plane bending vibrations δ(C-H) = 703 cm^{-1} of the styrene moieties. The spectra were treated with OMNIC 9 software. The function "atmosphere suppression" was applied to the full spectra. An automatic baseline correction was applied to facilitate the calculation of the α^{FTIR}. The formula used is:

$$\alpha^{FTIR}(t) = [I(t) - I_{min}] / [I_{max} - I_{min}] \quad (2)$$

where $I(t)$ is the band intensity on a spectrum at time t, I_{max} the maximal intensity recorded and I_{min} the minimal intensity (generally very close to 0). The intensities of the first recorded spectra were compared to that of the solvent at the same wavenumber. The noise was calculated in a wavenumbers range not presenting any band, through the corresponding function on the software. The signal-to-noise ratio was taken around 2 (which is below 3, the commonly used value), in order to ensure the detection of the very beginning of the phenomenon. These manipulations allowed to certify which was the first spectrum of a series that presented a band δ(C-H) = 703 cm^{-1}.

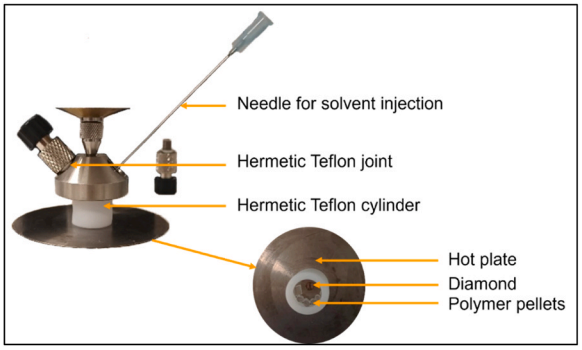

Fig. 1. Assembly for FTIR dissolution monitoring.

3.3. Differential scanning calorimetry

The identification of the glass transition behaviour was conducted with a Mettler Toledo DSC823 equipped with a HSS 8 + sensor. SAN pellets were introduced in triethyl citrate (20 %w/v SAN in TC, 15 h, 30 °C), then removed, excess of solvent was absorbed on a tissue, and a pellet was placed in a 100 μL aluminium crucible.

3.4. Thermogravimetric analysis (TGA)

The thermogravimetric analysis was used to calculate the percentage of completion of the dissolution for uncomplete dissolution in TC. Five SAN pellets (of about 17 mg each) were placed in five different vials, soaked with triethyl citrate (20 %w/v SAN in TC, 10 h, 45 °C), then taken out, excess of solvent was absorbed on a tissue, and the pellets were introduced in 70 μL alumina pans. The measurements were performed in a TGA 2 apparatus from Mettler-Toledo. The temperature ramp started from 25 °C to 600 °C with a heating rate of 10 °C/min, under a 60 mL/min air flow. The percentage of completion was calculated by subtracting the remaining SAN mass obtained after TC removal in TGA to the initial mass of the swollen pellet (TC+SAN) and dividing the result by the mass of the pellet before dissolution, followed by a multiplication by 100.

3.5. Optical microscopy

Microscopy images were taken using a ZEISS Axio Scope.A1 polarized light optical microscopy (POM) apparatus in reflection mode under a x10 zoom. The capture, treatment and analysis of the images were performed with Zen software. The SAN pellets were soaked in TC with methylene blue at 30 °C and 60 °C, overnight and for 20 mins respectively.

4. Theoretical section

4.1. Dissolution theory

The dissolution of a glassy polymer starts with the adsorption and the diffusion of the solvent in the bulk, which leads to the swelling of the polymer and the formation of a swollen layer where the polymer is still in the glassy state [28] (Fig. 2). Concomitantly, the polymer glassy-rubbery transition is induced by plasticization and results in the formation of a gel-like layer. Consequently, a gel-like swollen layer is formed. Once a critical concentration value of solvent in the polymer is reached, chain disentanglement can start. Those disentangled chains diffuse through a diffusion boundary layer (DBL) in the solvent. The swelling process continues as the disentanglement proceeds, until the bulk layer is completely transformed into a swollen layer. Dissolution

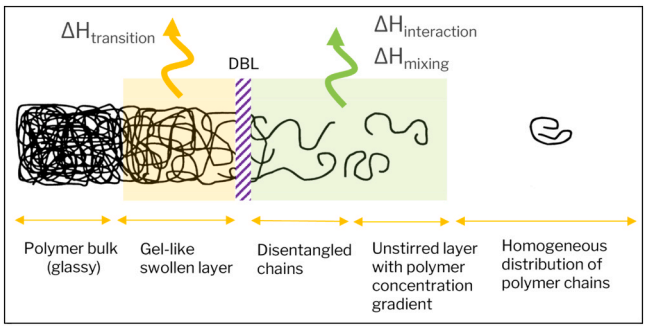

Fig. 2. Polymer dissolution mechanism through a diffusion boundary layer (DBL) and enthalpic contributions in case of an amorphous glassy polymer.

ends when all disentangled chains have diffused in the solvent [28,35].

The dissolution mechanism is limited either by the disentanglements or the diffusion of macromolecules [35]. It may also be controlled by the solvent diffusion rate and the swelling capacity, which depends on the size of the solvent molecule. The larger the solvent molecules, the more difficult it is for them to penetrate the polymer, thus slowing down the diffusion rate [36].

The overall enthalpic contribution for the dissolution of an amorphous glassy polymer is written as followed:

$$\Delta H_{\text{dissolution}} = \Delta H_{\text{transition}} + \Delta H_{\text{interaction}} + \Delta H_{\text{mixing}} \tag{3}$$

with $\Delta H_{\text{transition}}$ associated with the chain relaxation during the glassy-rubbery transition [37], $\Delta H_{\text{interaction}}$ is referring to the new polymer-solvent interactions, and ΔH_{mixing} corresponds to the macromolecule disentanglement and rearrangement of conformation [38].

4.2. Hansen theory

The polymer solubility in solvents may be predicted according to the Hansen model [39], which takes into account the dispersive forces, the polar cohesive forces and the hydrogen bonding, characterized by δ_D, δ_P, and δ_H components, respectively [28].

The solubility parameter distance is described as follows:

$$R_a^2 = 4 \quad (\delta_{D,2} - \delta_{D,1})^2 + \quad (\delta_{P,2} - \delta_{P,1})^2 + \quad (\delta_{H,2} - \delta_{H,1})^2 \tag{4}$$

With 1 and 2 being the notations for solvent and polymer contributions, respectively.

The relative energy difference (RED) is calculated as follows:

$$RED = \quad \frac{R_a}{R_0} \tag{5}$$

with R_0 the sphere interaction radius related to the polymer. If RED < 1, the solvent is in the Hansen sphere and solvent-polymer interactions are favourable enough to promote the dissolution, contrary to a RED exceeding 1.

Based on the Hansen solubility parameters found in the literature, the Hansen sphere of the SAN was plotted together with the Hansen coordinates of two solvents (Figure S1). The sphere interaction radius of the SAN is $R_0 = 4.80$ [39]. Diethyl succinate (DS) is located within the SAN sphere and can be considered as a good solvent for SAN dissolution. This solvent has a RED close to that of the MEK (RED = 0.60). Diethyl succinate is then expected to have similar dissolution power. On the other hand, triethyl citrate (TC) is outside the SAN sphere and was selected as a poor solvent for SAN dissolution. It was used to broaden the scope of the study. When conducting thermodynamic studies, particularly above the glass transition temperature of SAN (T_g = 107 °C), high-boiling solvents should be selected. All chosen solvents meet this criterion. In general, increasing temperature induces a widening of the solubility sphere and a decrease in HSP. δ_H is the most impacted parameter. Consequently, when increasing temperature, alcoholic solvents' ability to dissolve polymers with lower HSP is heightened. Thus, poor solvents may become good solvents at higher temperatures. [39] The RED values at 25 °C, determined through Eqs. (1) and (2), and the boiling temperature of the selected solvents are gathered in Table 1 along with the RED values at 120 °C. Those latter were calculated according to **Equations** [39] **(S1)**, **(S2)** and **(S3)** which were reported in supporting information. The recalculated HSP of the SAN and the solvents were reported in Table S1.

4.3. Isoconversional kinetics

Kinetic processes occurring in condensed phases may be investigated using the corresponding general form for the rate equation formulated as [41]:

$$\frac{d\alpha}{dt} = k(T)f(\alpha) = A\exp\left(-\frac{Ea}{RT}\right)f(\alpha) \tag{6}$$

with α the extent of conversion, t the time, $k(T)$ the rate constant which follows the Arrhenius law, $f(\alpha)$ the model of the reaction standing for the reaction mechanism, A the pre-exponential factor, E_a the activation energy, R the universal gas constant, and T the absolute temperature. Multiple kinetic models were developed and reported in the literature [42].

Chemical processes and physical transformations may be studied through isothermal and non-isothermal calorimetric measurements. To get an insight on the progression of the phenomenon, the extent of conversion may be calculated from the recorded data using Eq. (7):

$$\alpha_i = \frac{\int_{t_1}^{t_i}(dH/dt)_i dt}{\int_{t_1}^{t_2}(dH/dt)_i dt} \equiv \frac{H_i}{Q} \tag{7}$$

With $(dH/dt)_i$ being the heat flow recorded by the calorimeter at time i (t_i). Lower and upper integration limits are respectively set at time t_1 and t_2 on the calorimetric signal. The reaction rate $(d\alpha/dt)$ can be obtained by calculating the derivative of Eq. (7).

Friedman method is part of the earliest proposed isoconversional kinetic methods and is described with the Eq. (8) which ensues from Eq. (6) linearization [43]:

$$\ln\left(\frac{d\alpha}{dt}\right)_{\alpha,i} = \ln[A_\alpha f(\alpha)] - \frac{E_a}{RT_{\alpha,i}} \tag{8}$$

where the index i designates the temperature used by the program and α stipulates that computations are carried out for a constant value of the extent of conversion.

Herein, the advanced non-linear isoconversional method (NLN) established by Vyazovkin [44–46] was used. The corresponding equations are derived from Eq. (6) and written as follows:

$$\Phi(E_a) = \quad \sum_{i=1}^{n}\sum_{j\neq i}^{n}\frac{J[E_a, T_i(t_\alpha)]}{J[E_a, T_j(t_\alpha)]} \tag{9}$$

Table 1
SAN and solvents Hansen solubility parameters at 25 °C, RED at 25 °C and 120 °C and solvents boiling temperatures.

	Hansen solubility parameters ($MPa^{1/2}$)					
	δ_D (25 °C)	δ_P (25 °C)	δ_H (25 °C)	RED (25 °C)	RED (120 °C)	B.T (°C)
SAN [39]	16.6	9.8	7.6			
Diethyl succinate (DS) [40]	16.2	6.8	8.7	0.69	0.79	218
Triethyl citrate (TC) [39]	16.5	4.9	12	1.37	2.00	294

where the function $J[E_\alpha, T_i(t_\alpha)]$ is expressed as:

$$J[E_a, T(t_\alpha)] \equiv \int_{t_\alpha-\Delta\alpha}^{t_\alpha} \exp\left[\frac{-E_a}{RT(t)}\right] dt \quad (10)$$

This NLN method uses a series of temperature programs $T_i(t)$ and was executed using a internally generated software [47–49]. $\Phi(E_a)$ is minimized for each value of α and a dependency of the effective activation energy (E_a) on the extent of conversion (α) may be plotted. This method does not require any assumptions about the reaction mechanism. The resulting E_a dependencies enable meaningful mechanistic analyses and improve the knowledge on multiple-step processes [42,50,51]. In most cases, E_a computations via NLN and Friedman methods provide similar results. Then E_a variations may be attributed to rate-determining step changes over the studied process.

The rate constant $k_\alpha(t)$ dependency on α is computed according to Eq. (11), using previously calculated E_a and A_α variations:

$$k_\alpha(t) = A_\alpha \exp\left(-\frac{E_a}{RT}\right) \quad (11)$$

Next step is the calculation of the reaction model function $f(\alpha)_\alpha$ following the equation:

$$f(\alpha)_\alpha = \frac{(d\alpha/dt)_\alpha}{k_\alpha} \quad (12)$$

5. Results and discussion

The dissolution of SAN was monitored in both diethyl succinate and triethyl citrate by reaction calorimetry. Calorimetric experiments were performed below and above the glass transition temperature of SAN (T_g = 105 °C, see Figure S2) to study the influence of the polymer state on its dissolution. Isothermal temperatures ranging from 30 °C to 150 °C were chosen, and the respective extents of conversion $\alpha^{CAL}(t)$ are plotted against time in Figure S3 for the dissolution of SAN in DS. As expected, the higher the temperature, the faster the dissolution. To compare the phenomenon below and above T_g, the heat flow curves recorded at 45 °C and 120 °C are presented respectively in (Fig. 3 **(a)**) and (Fig. 3 **(b)**). The obtained dissolution enthalpies after integration of the heat flow curves are summarized in Fig. 4.

The total enthalpic contribution (independently of the solvent) is exothermic over the whole range of temperature, which is consistent with the literature [52].

The higher the enthalpy of dissolution is, the more efficient the solvent is [38]. Here in, the enthalpy values correlate with the HSP predicted affinities of the solvents for the polymer. As shown in Fig. 4, the good solvent (DS) presents higher values of enthalpy compared to TC when the dissolution occurs below the T_g of SAN.

First, complete dissolution was observed for the SAN/DS system

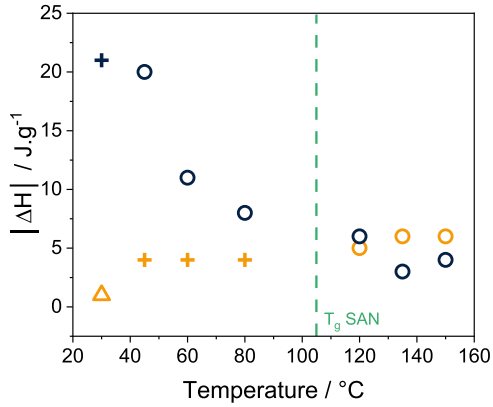

Fig. 4. Enthalpies associated with the dissolution of SAN (at 30, 45, 60, 80 and 120, 135 and 150 °C) in diethyl succinate (black) and triethyl citrate (orange). After 15 h, no dissolution (triangle), partial dissolution (cross) or complete dissolution (round) were observed.

(20 %w/v) for temperatures higher than 45 °C. The absolute value of the enthalpic contribution of SAN dissolution in diethyl succinate is of 20 J/g at 45 °C and progressively decreases when temperature increases to reach about 6 J/g at 120 °C. This is coherent with the fact that the $|\Delta H_{Tg}|$ decreases when the temperature tends towards the T_g of SAN. $|\Delta H_{Tg}|$is expected to be about 0 J/g when $T \geq T_g$. Above T_g, $\Delta H_{dissolution}$ = 6 J/g, in accordance with the fact that ΔH_{Tg} is not predominant and that the dissolution at least is not governed by the glassy-rubbery transition. Then, the total enthalpy measured above T_g is attributed to $\Delta H_{interaction}$ + ΔH_{mixing} = 6 J/g. It confirms that below T_g, the heat released during dissolution is then predominated by $\Delta H_{transition}$ that should be around 14 J/g.

Conversely, the dissolution of SAN in TC (20 %w/v) does not occur after 20 h at 30 °C. Indeed, when monitoring the dissolution by FTIR, no band attributed to SAN appears on the spectrum (Figure S4). This implies that no macromolecules diffused in solution and that the polymer did not dissolve. The dissolution process could be observed via interferometry [30]. Herein, no gel-like layer could be seen besides the bulk when observing the pellet by microscopy after soaking (Figure S5 **(a)**), whereas the gel-like layer was observed when the pellet was previously dissolved in TC at 60 °C (Figure S5 **(b)**). This is supported by the calorimetry. The total measured enthalpic contribution of the SAN in TC, (after 15 h at 30 °C) is only 1 J/g (Fig. 4), which leads to the conclusion that the polymer did not undergo a complete glassy-rubbery transition (as for SAN in DS) and consequently no dissolution. However, the occurrence of some swelling and solvent penetration after 15 h of dissolution at 30 °C can be deduced from the DSC scan (Figure S2). Indeed, a glass transition of a swollen layer of SAN appeared in the DSC

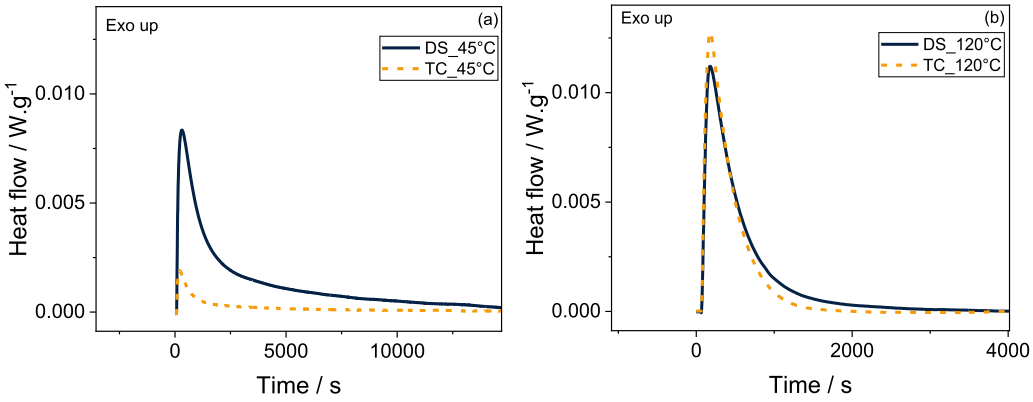

Fig. 3. Heat flow curves for the dissolution of SAN (20 %w/v polymer in solvent, 15 h) at (a) 45 °C in diethyl succinate (DS) (black line) and in triethyl citrate (orange dash line) and (b) 120 °C in diethyl succinate (DS) (black line) and in triethyl citrate (orange dash line).

scan just below the glass transition of the bulk SAN. Moreover, the solvent that was used to soak the pellets before the DSC measurement was analysed in FTIR. No band associated to SAN polymer was observed, confirming that no dissolution occurred. So, the polymer did undergo a partial swelling via diffusion of some TC but not leading to a rubbery state at 30 °C allowing for chain disentanglement and solubilisation. This confirms that the transition from the glassy to the rubbery state limits the dissolution. It is in accordance with the dissolution mechanism described in the literature which depicts the progressive formation of swollen and gel-like layers, as the glassy bulk layer is progressively disappearing [28].

When performing SAN dissolution in TC at 45 °C, 60 °C and 80 °C, the polymer is partly dissolved (Fig. 4) and the enthalpic contribution increases to 4 J/g. At 120 °C, above the T_g(SAN), the dissolution in TC is complete and the enthalpy is in the same order of magnitude (~ 6 J/g) as for DS (Fig. 4). Considering the ± 1 % precision interval, no significant drop in the global enthalpy is observed when the temperature is above T_g(SAN) as was the case for DS. As for dissolution in DS, ΔH_{Tg} is not contributing above T_g(SAN) and the measured enthalpy correspond to $\Delta H_{interaction} + \Delta H_{mixing}$. As shown in Fig. 3**(b)**, the heat flow curves of SAN dissolution - measured for temperatures above T_g - are similar for both TC and DS.

Also, the molar volumes of DS and TC are V_m(DS) = 167 mL/mol and V_m(TC) = 242 mL/mol respectively. It was reported that solvents with a larger molar volume imply higher free energy of mixing which reduces the miscibility, and thus slow down the dissolution of polymers [28,39]. Indeed, Papanu et al. [53] reported drastic drops of the solvent penetration rate in PMMA with small increase of the molar volume. Hence, the larger molar volume of TC could also influence its poor solvency below T_g(SAN).

If the dissolution step supplies an exothermic enthalpy between 6 J·g^{-1} (0.006 kJ·g^{-1}) and 20 J.g^{-1} (0.02 kJ.g^{-1}), this heat can be partially or fully recovered to offset the external thermal energy required for solvent evaporation. Considering 1 kg of SAN (feedstock), Table 2 summarizes the estimated net external thermal energy required for evaporation of 5 kg of diethyl succinate (DS) or triethyl citrate (TC), i.e. 20 wt% of SAN in solvent, considering only latent heat (0.314 kJ.g^{-1} for DS and 0.247 kJ.g^{-1} for TC) and a high-efficiency solvent recovery scenario (recovery rate 99.8 %). The solvent losses are assumed to be 2 kg per metric ton of feedstock (SAN). Solvent losses consist of residual solvent in the product and general process losses (micro leaks). The calculations assume an evaporation penalty of 120 % of the ideal latent heat and a condenser heat recovery of 50 %, resulting in a net external latent requirement of 60 % of the ideal ΔH_{vap}. Table 2 further accounts for a range of possible exothermic contributions from the dissolution process steps (range 6–20 J·g^{-1}), with heat capture efficiencies η = 0 (no capture), 0.5 (50 % captured), and 1.0 (100 % captured). The resulting ranges of net external energy (kJ and kWh) illustrate how even modest exothermic process heats can reduce the energy burden by ~3–13 %, depending on exotherm magnitude and capture efficiency. Table 2 is intended only to provide a rough quantitative overview of solvent recovery operations.

The polymer dissolution in DS was also monitored by FTIR. The δ(C-H)$_{styrene}$ = 703 cm^{-1} was selected as the band to be followed (Fig. 5) because it was the only band sufficiently intense, free of overlap or overshouldering from the solvent. The full spectra with inserted zooms can be found in the supporting information (Figure S6) as well as the diethyl succinate spectrum (Figure S7). SAN bands attribution was made based on the literature [54,55] and can be found in Table S2.

Fig. 5 depicts FTIR spectra measured during the SAN dissolution in DS at 45 °C. The intensity of the band increases over dissolution time until it reaches a plateau.

The associated FTIR extent of conversion is shown in Fig. 6**(a)** and it shows good correlation together with the extent of conversion obtained by calorimetry. The heat flow curves and the corresponding extent of conversion refers to an overall heat of dissolution with no distinction between the swelling, transition, disentanglement, and diffusion of polymer macromolecules in solvent. On the other hand, FTIR solely detects vibrations of macromolecules once they are in solution. Consequently, the zoom on the FTIR extent of conversion at short times (Fig. 6 **(a)**) highlights the time it takes for the polymer chains to begin diffusing in the solvent. For the first points, when intensity equals 0 (i.e induction period), only swelling, transition, disentanglement are proceeding. Then, the first macromolecules in solvent appear when intensity value exceeds 0.

At 45 °C, the diffusion of SAN in DS starts after 480 s Fig. 6**(a)**). Conversely, the time needed for SAN chains to start diffusing in TC at 45 °C is much longer, around 5000 s (Fig. 6**(b)**). Such long induction periods were reported for the sorption of methanol in poly(methyl methacrylate) (2.5 h) [56]. This could be caused by a slow glassy-rubbery transition in poor solvent. The appearance of an induction period was already identified in the literature for the dissolution of polymers at temperatures below their T_g [57,58], using techniques such as refractometry [59], viscometry [58], ellipsometry [60] and UV-spectrophotometry [61] to monitor *in situ* the dissolution (except for UV-spectrophotometry). These studies were conducted on a restricted temperature range. The induction period to the first detection of polymer chains in solvent decreases when temperature [56–58] increases and becomes minimal for temperatures around the T_g [57].

When increasing the temperature up to 120 °C (Fig. 7), that induction period decreases down to 120 s for DS (Fig. 7**(a)**). 5-seconds-short induction period was reported for the dissolution of poly(oxetane) in its rubbery state [61]. In TC, when $T > T_g$(SAN) the induction period falls to 360 s (Fig. 7**(b)**), which is three times the value obtained in DS. It is postulated that the induction period decreases because no glassy-rubbery transition occurs above T_g. Moreover, it is not clear in the literature [36] whether the glassy-rubbery transition governs the dissolution or may be neglected. Herein, it is demonstrated that in the case of the dissolution of SAN in DS and TC, the glassy-rubbery transition governs the dissolution below T_g but not above T_g.

Table 2
Net external energy for evaporating 5 kg of DS or TC (latent heat only, 60 % net) with exothermic contributions of 6–20 J·g^{-1} at varying capture efficiencies (η = 0, 0.5, 1.0), in kJ and kWh.

Solvent	Exotherm (J/g)	Capture η	Net External Energy (kJ)	Net External Energy (kWh)
DS	6–20	0	940.8	0.2613
	6–20	0.5	880.8 – 922.8	0.2447 – 0.2563
	6–20	1.0	820.8 – 904.8	0.2280 – 0.2513
TC	6–20	0	740.70	0.2058
	6–20	0.5	680.70 – 722.70	0.1891 – 0.2007
	6–20	1.0	620.70 – 704.70	0.1724 – 0.1957

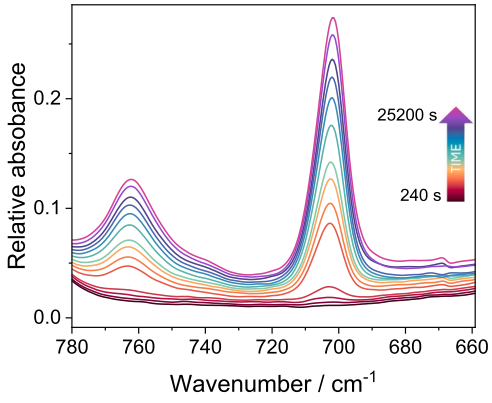

Fig. 5. FTIR spectra for the dissolution monitoring of SAN pellets in diethyl succinate (20 %w/v) at 45 °C. Zoom on the δ(C-H)$_{styrene}$ bands at 703 cm^{-1} and 764 cm^{-1}. For a better legibility, spectra were translated along Y axis.

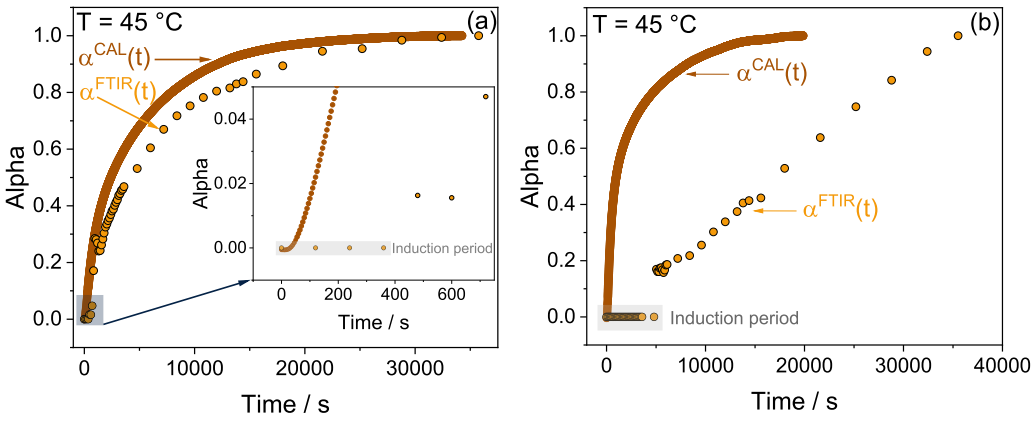

Fig. 6. Calorimetric extent of conversion $\alpha^{CAL}(t)$ (brown) and FTIR extent of conversion $\alpha^{FTIR}(t)$ (orange) for the dissolution of SAN at 45 °C in (a) diethyl succinate (20 %w/v) and (b) triethyl citrate (20 %w/v). Inset: zoom on the extents of conversion.

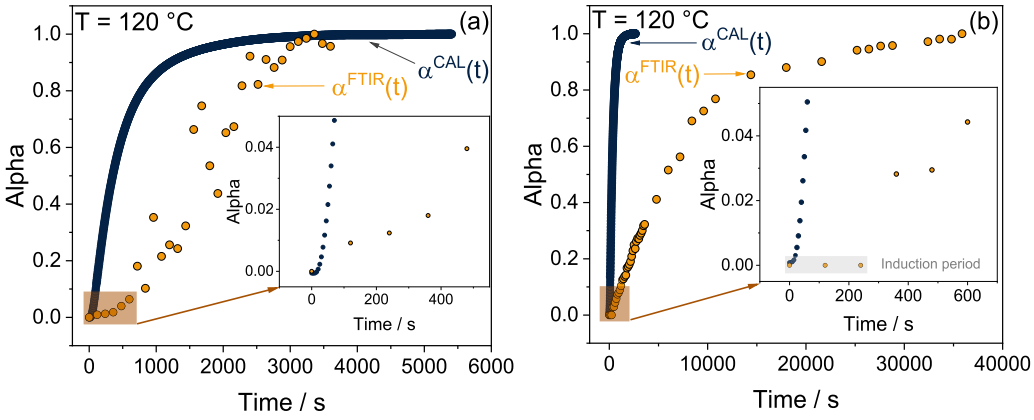

Fig. 7. Calorimetric extent of conversion $\alpha^{CAL}(t)$ (black) and FTIR extent of conversion $\alpha^{FTIR}(t)$ (orange) for the dissolution of SAN at 120 °C in (a) diethyl succinate (20 %w/v) and (b) triethyl citrate (20 %w/v). Insets: zoom on the extents of conversion.

In isothermal calorimetry the heat flow returns to the baseline and becomes negligeable before dissolution completes, no matter the temperature. Consequently, α^{CAL} could be considered as a relative extent of conversion.

SAN pellets were also dissolved in vials and taken out at different times to be visually observed. From this, it appeared that the dissolution of SAN in TC at 45 °C for 10 h was unfinished. The corresponding percentage of completion after 10 h in TC was calculated from TGA measurements on the swollen pellets (giving the amount of remaining SAN mass) and it gives $\%_{completion} = 21.6\ \%$. Then, α^{FTIR} is not absolute because, unfortunately, running experiments for more than 10 h is not feasible and dissolution is not finished yet. Complete dissolution of SAN in TC required 11 days to be completed at 45 °C, compared to only 9 h at 120 °C. In DS, dissolution was complete after 14 h at 45 °C and 6.5 h at 120 °C.

Anyway, when coupling the calorimetry with the FTIR monitoring, it seems possible to discriminate between good and poor solvents for the polymer dissolution by comparing the respective alpha. If the two extents of conversion are well correlated, the solvent could be considered as favourable for the dissolution. In the case of a poor solvent for the dissolution, the slopes tend to differ (i.e. the correlation is not good). In fact, the enthalpic phenomenon is then only a small contribution to the global phenomenon. The solvent may not have enough affinity with the polymer to efficiently promote its dissolution. Moreover, in this study, the Hansen theory does not correctly predict the solvent-polymer affinity at high temperature. Indeed, according to the calculations at 120 °C, the RED values increase with temperature (Table 1), whereas it was demonstrated that the dissolution of SAN was thermodynamically furthered in both DS and TC.

5.1. Isoconversional kinetic treatment of the calorimetric measurements

As shown in Fig. 8, the kinetic analysis of SAN dissolution reveals a multi-step process with distinct rate-limiting factors depending on whether dissolution occurs below or above the SAN glass transition temperature (T_g).

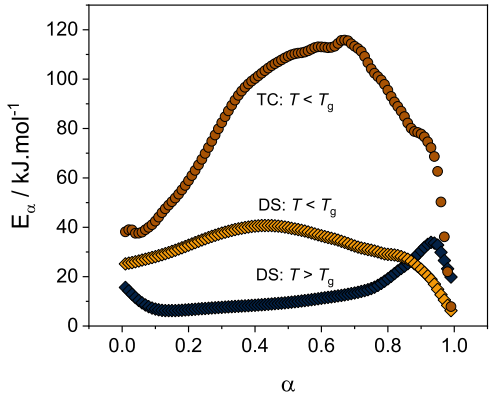

Fig. 8. Variation of the effective activation energy (E_a) with the extent of conversion (α) for the dissolution of SAN in DS below T_g (orange), above T_g (black) and in TC below T_g (brown), respectively computed at 30/45/60/80 °C; 120/135/150 °C and 45/60/70/80 °C.

When a polymer is exposed to a solvent, molecular diffusion and chain relaxation dictate the dissolution process. In the rubbery state (above T_g), polymer chain mobility is high, making solvent diffusion the rate-limiting step. This is classified as Fickian diffusion. [62–64] The effective activation energy (E_a) corresponds to the variation of the activation energy of the total phenomenon of dissolution (which englobes solvent diffusion, disentanglement and chain diffusion), for each value of the conversion. The activation energy (E_a) observed for SAN dissolution in DS above T_g (Fig. 8) falls within the range of 6–15 kJ/mol, aligning with typical diffusion-controlled processes. It may be associated with the process of small molecules diffusion. [47] Or for instance, the dissolution of poly(oxetane) in ethyl acetate reported a value of 14 kJ/mol for the activation energy for the diffusion of the macromolecular chains through the boundary layer [61]. As detailed in Appendix 1, the reptation regime (from the Doi-Edwards reptation equation) is not relevant for a 20 %wt solution of SAN in DS at 120 °C. The chain relaxation in the DS solution is rather corresponding to a disentangled regime (Rouse/Zimm).

For $\alpha < 0.10$, a E_a decrease is observed. In chemical reactions, this decrease is often attributed to a catalytic effect, where the reaction initially proceeds slowly but becomes increasingly facilitated as the process advances. Similarly, in dissolution processes, we observe that the initial stage occurs less easily, with the rate of dissolution accelerating thereafter. At $0.1 < \alpha < 0.6$, a contribution from long-chain diffusion leads to an increase in E_a. As solvent molecules permeate the polymer, they create voids in the matrix, raising E_a at $\alpha > 0.60$ [59]. The final drop in E_a from 34 to 20 kJ/mol suggests a return to solvent diffusion control.

For dissolution below T_g, the kinetic profile differs significantly. The values obtained for $\alpha < 0.85$ are always higher than the values obtained for SAN dissolution in DS above T_g, which is consistent with the lower mobility below T_g. Solvent diffusion typically exhibits E_a values between 10 and 20 kJ/mol [47]. However, SAN dissolution below T_g shows an E_a increase from 25 to 41 kJ/mol for $0.10 < \alpha < 0.43$, indicating a combination [51,65] of solvent diffusion and segmental relaxations (Fig. 8). This phenomenon, known as Case II diffusion, is characterized by macromolecular segmental relaxations limiting dissolution. [63,64,66] Swelling activation energies for PVC dissolution in cyclohexane were around 36 – 56 kJ/mol [57]. Activation energies for such relaxations are higher than those for simple diffusion. [62] The transition from glassy to rubbery states, induced by solvent plasticization, is thus reflected in a rise in E_a. Initially, below T_g, dissolution of SAN in DS is controlled by segmental relaxation up to $\alpha = 0.43$ (Fig. 8). Beyond this point, E_a drops to 29 kJ/mol, signifying a shift to solvent diffusion control, though segmental relaxations persist. The sharp decline to 6 kJ/mol at $\alpha > 0.80$ suggests that chain relaxations cease and dissolution is fully solvent diffusion-driven [47]. This aligns with enthalpic findings, where $\Delta H_{transition}$ dominates $\Delta H_{dissolution}$ below T_g but becomes negligible above T_g. The obtained E_a values are also comparable to those reported for polymer chain disentanglement (15–60 kJ/mol). [67] However, if dissolution were solely controlled by chain disentanglement, E_a trends would be similar above and below T_g, which is not observed in Fig. 8.

Further kinetic analysis below T_g supports these conclusions. The function $f(\alpha)_\alpha$ (Figure S8) suggests Case I diffusion dominates for $0.44 \leq \alpha \leq 1$, while deviations for $\alpha < 0.44$ indicate an additional limiting process, segmental relaxation, reinforcing the Case II mechanism. Due to overlapping α curves, the $f(\alpha)_\alpha$ analysis was not feasible for dissolution above T_g.

In TC, SAN dissolution is partial, with E_a trends resembling those in DS below T_g but at higher values (Fig. 8). This is consistent with the lower ability of TC to dissolve the polymer chains. E_a increases from 39 to 116 kJ/mol over $0.07 < \alpha < 0.68$, which is consistent with Case II diffusion (96–155 kJ/mol for PMMA in acetone-based solvents [60]). These elevated values indicate a stronger segmental relaxation limitation. Compared to DS, the broader α range of E_a increase further highlights the dominance of segmental relaxations over solvent diffusion. This interpretation aligns with FTIR, and calorimetric results for SAN dissolution in TC at 30°C.

For $0.68 < \alpha < 0.90$, E_a decreases from 116 to 78 kJ/mol, indicating a transition to solvent diffusion control. At $\alpha > 0.90$, dissolution is entirely solvent-diffusion limited, with E_a dropping from 78 to 8 kJ/mol. This final E_a value is higher than in DS, likely due to incomplete dissolution, suggesting higher temperatures would be required to reach process completion.

Above T_g in TC, the similarity of α curves (Fig. 9) and their cross-over (zoom on Fig. 9) between the different temperatures hindered the isoconversional kinetic treatment, implying that dissolution is thermodynamically driven rather than kinetically driven (i.e. independent from temperature).

The dissolution rates (Figure S9) show that in DS at 120°C, the maximum dissolution rate is three times that in DS at 60°C and four times that in TC at 60°C, confirming temperature effects on dissolution kinetics.

The influence of the thickness of SAN pieces on the E_a for the dissolution in DS below T_g (Fig. 10) was also investigated. The concentration was unchanged. The computed E_a were compared to that of the dissolution of the pellets. The general variation of E_a with α remained the same. The E_a reached 50 kJ/mol at $\alpha = 0.41$ for a thickness of 1.36 mm, and 74 kJ/mol at $\alpha = 0.45$ for a thickness of 4.08 mm, compared to 41 kJ/mol at $\alpha = 0.43$ for the pellets. Hence, it is observed that a higher thickness (or a lower specific surface area) induces a stronger limitation by the segmental relaxations and a slowing down of the dissolution rate, of the SAN samples.

In summary, SAN dissolution kinetics involve a transition between rate-limiting steps depending on temperature. Below T_g, segmental relaxation governs the initial phase, transitioning to solvent diffusion at higher α. Above T_g, dissolution is primarily diffusion-limited.

6. Conclusions

This study provides critical insights into the temperature dependence of SAN dissolution, laying the groundwork for advancing ABS physical recycling via dissolution/precipitation technologies. By enabling *in situ* monitoring of SAN dissolution, these findings offer a pathway to optimize polymer recovery processes.

The use of high-boiling point solvents allowed the investigation of SAN dissolution both below and above T_g, covering a broad temperature range and facilitating comparisons between good (DS) and poor (TC) solvents from both thermodynamic and kinetic standpoints. Calorimetric measurements revealed that the enthalpy of dissolution is primarily dominated by ΔH_{Tg}. When dissolution occurs above T_g, the absence of a glassy-rubbery transition leads to minimal segmental

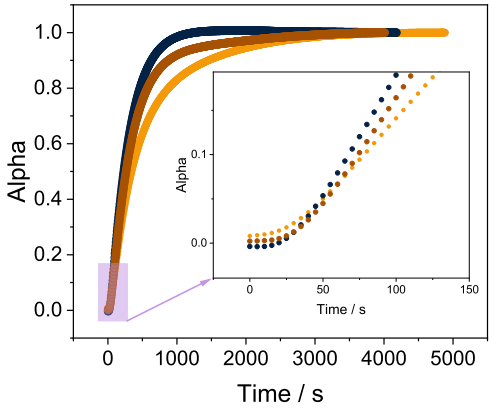

Fig. 9. Calorimetric extent of conversion $\alpha^{CAL}(t)$ for the dissolution of SAN in triethyl citrate (20 %w/v) at 120 °C (black), 135 °C (brown) and 150 °C (orange). Inset: zoom on the extents of conversion.

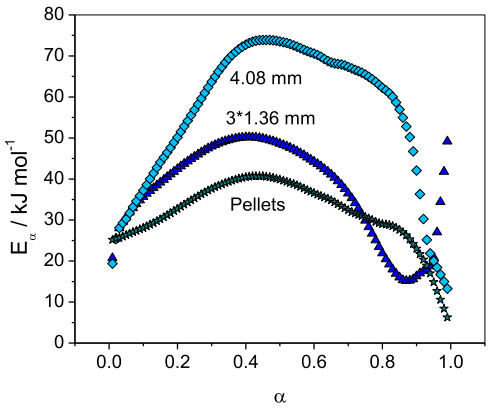

Fig. 10. Variation of the effective activation energy (E_a) with the extent of conversion (α) for the dissolution of SAN in DS below T_g, at 45/60/75/90 °C for the pieces of 1.36 mm (navy blue) and 4.08 mm (light blue) of thickness, and 45/60/70/80 °C for the pellets (green).

relaxation contributions, with the dominant factors being $\Delta H_{interaction}$ and ΔH_{mixing}. This results in a shortened induction period, as observed through ATR-FTIR spectroscopy. The induction period represents the time required for polymer chains to initiate diffusion into the solvent, during which swelling, transition, and disentanglement occur. The prolonged induction period in TC below T_g is likely due to the stronger limiting effect of segmental relaxations.

The kinetics of SAN dissolution is a multi-step process governed by distinct rate-limiting steps depending on whether the polymer starts in a glassy or rubbery state. Above T_g, dissolution follows a diffusion-limited mechanism consistent with Fickian diffusion, while below T_g, it is controlled by both solvent diffusion and segmental relaxation, characteristic of Case II diffusion. The choice of solvent and temperature plays a crucial role in determining dissolution efficiency, with DS enabling faster and more complete dissolution compared to TC.

These findings offer valuable insights for enhancing polymer dissolution methods in advanced physical recycling processes. Specifically, they highlight the critical importance of considering whether dissolution occurs above or below the polymer's T_g, as this significantly impacts the dissolution kinetics. By taking these temperature-dependent differences into account, recycling techniques can be optimized for greater efficiency and effectiveness.

CRediT authorship contribution statement

Giuseppe Melilli: Visualization, Validation, Methodology, Investigation, Conceptualization. **Luc Vincent:** Writing – review & editing, Validation, Supervision, Methodology, Data curation, Conceptualization. **Mark C.P. Roelands:** Validation, Resources, Funding acquisition, Conceptualization. **Ruud Cuypers:** Writing – review & editing, Visualization, Validation, Project administration, Conceptualization. **Pieter Janssen:** Writing – review & editing, Visualization, Validation, Methodology, Conceptualization. **Andreia. F. Sousa:** Writing – review & editing, Visualization, Validation, Methodology. **Nicolas Sbirrazzuoli:** Writing – review & editing, Validation, Supervision, Software, Data curation, Conceptualization. **Nathanael Guigo:** Writing – review & editing, Validation, Supervision, Project administration, Methodology, Funding acquisition, Conceptualization. **Sandra Litwin:** Writing – original draft, Methodology, Investigation, Formal analysis, Data curation.

Funding

European Commission, grant no. 101058636.

Declaration of Competing Interest

The authors declare the following financial interests/personal relationships which may be considered as potential competing interests: Nathanael Guigo reports financial support was provided by European Commission. If there are other authors, they declare that they have no known competing financial interests or personal relationships that could have appeared to influence the work reported in this paper

Acknowledgements

The authors express their gratitude to the European Health and Digital Executive Agency (HADEA) under the power delegated by the European Commission for its support of the project ABSolEU — 'Paving the way for an ABS recycling revolution in the EU'. The authors also acknowledge CICECO-Aveiro Institute of Materials under the projects UIDB/50011/2020 (DOI 10.54499/UIDB/50011/2020), UIDP/50011/2020 (DOI 10.54499/UIDP/50011/2020) & LA/P/0006/2020 (DOI 10.54499/LA/P/0006/2020), financed by national funds through the FCT/MCTES (PIDDAC). The FCT is acknowledged for the research contract to AFS (CEECINSTLA/00002/2022).

Appendix A. Supporting information

Supplementary data associated with this article can be found in the online version at doi:10.1016/j.mtcomm.2025.114556.

Data availability

Data will be made available on request.

References

[1] Recycling of Plastics - Hanser Publications. ⟨https://www.hanserpublications.com/Products/634-recycling-of-plastics.aspx⟩ (accessed 2024-01-15).
[2] E.-K. Karahaliou, P. a Tarantili, Stability of ABS compounds subjected to repeated cycles of extrusion processing, Polym. Eng. Sci. 49 (11) (2009) 2269–2275, https://doi.org/10.1002/pen.21480.
[3] I. Hamarat, E. Kuram, B. Ozcelik, Investigation the mechanical, rheological, and morphological properties of acrylonitrile butadiene styrene blends with different recycling number content, Proc. Inst. Mech. Eng. Part E J. Process Mech. Eng. 232 (4) (2018) 449–458, https://doi.org/10.1177/0954408917717994.
[4] M. Rahimi, M. Esfahanian, M. Moradi, Effect of reprocessing on shrinkage and mechanical properties of ABS and investigating the proper blend of virgin and recycled ABS in injection molding, J. Mater. Process. Technol. 214 (11) (2014) 2359–2365, https://doi.org/10.1016/j.jmatprotec.2014.04.028.
[5] T. Uekert, A. Singh, J.S. DesVeaux, T. Ghosh, A. Bhatt, G. Yadav, S. Afzal, J. Walzberg, K.M. Knauer, S.R. Nicholson, G.T. Beckham, A.C. Carpenter, Technical, economic, and environmental comparison of closed-loop recycling technologies for common plastics, ACS Sustain. Chem. Eng. 11 (3) (2023) 965–978, https://doi.org/10.1021/acssuschemeng.2c05497.
[6] J. Jiang, K. Shi, X. Zhang, K. Yu, H. Zhang, J. He, Y. Ju, J. Liu, From plastic waste to wealth using chemical recycling: a review, J. Environ. Chem. Eng. 10 (1) (2022) 106867, https://doi.org/10.1016/j.jece.2021.106867.
[7] I. Vollmer, M.J.F. Jenks, M.C.P. Roelands, R.J. White, T. van Harmelen, P. de Wild, G.P. van der Laan, F. Meirer, J.T.F. Keurentjes, B.M. Weckhuysen, Beyond mechanical recycling: giving new life to plastic waste, Angew. Chem. Int. Ed. 59 (36) (2020) 15402–15423, https://doi.org/10.1002/anie.201915651.
[8] Y.-B. Zhao, X.-D. Lv, H.-G. Ni, Solvent-based separation and recycling of waste plastics: a review, Chemosphere 209 (2018) 707–720, https://doi.org/10.1016/j.chemosphere.2018.06.095.
[9] E.M. Kampouris, C.D. Papaspyrides, C.N. Lekakou, A model process for the solvent recycling of polystyrene, Polym. Eng. Sci. 28 (8) (1988) 534–537, https://doi.org/10.1002/pen.760280808.
[10] J.G. Poulakis, P.C. Varelidis, C.D. Papaspyrides, Recycling of polypropylene-based composites, Adv. Polym. Technol. 16 (4) (1997) 313–322, https://doi.org/10.1002/(SICI)1098-2329(199711)16:4<313::AID-ADV5>3.0.CO;2-Y.
[11] D. Arends, M. Schlummer, A. Mäurer, Removal of inorganic colour pigments from acrylonitrile butadiene styrene by dissolution-based recycling, J. Mater. Cycles Waste Manag 14 (2) (2012) 85–93, https://doi.org/10.1007/s10163-012-0041-5.
[12] K.F. Drain, W.R. Murphy, M.S. Otterburn, A solvent technique for the recycling of polypropylene — degradation on recycling, Conserv. Recycl 6 (3) (1983) 123–137, https://doi.org/10.1016/0361-3658(83)90036-X.
[13] A. Mäurer, M. Schlummer, Good as New. Recycling plastics from WEEE and packaging waste, Waste Manag. World 3 (2004) 33–43.

[14] M. Schlummer, A. Mäurer, T. Leitner, W. Spruzina, Report: recycling of flame-retarded plastics from waste electric and electronic equipment (WEEE), Waste Manag. Res. 24 (6) (2006) 573–583, https://doi.org/10.1177/0734242X06068520.

[15] CÔTÉ, R. Processes for Recycling Polystyrene Waste. WO2016049782A1, April 7, 2016. ⟨https://patents.google.com/patent/WO2016049782A1/en⟩ (accessed 2024-11-05).

[16] Z. Kara Ali, J.-M. Pin, C. Pellerin, Quantification of P-Cymene and heptane in a solvent-based green process of polystyrene recycling, Appl. Spectrosc. Pr. 1 (1) (2023) 27551857231179982, https://doi.org/10.1177/27551857231179982.

[17] J.-M. Pin, I. Soltani, K. Negrier, P.C. Lee, Recyclability of post-consumer polystyrene at pilot scale: comparison of mechanical and solvent-based recycling approaches, Polymers 15 (24) (2023) 4714, https://doi.org/10.3390/polym15244714.

[18] Layman, J.M.; Gunnerson, M.; Bond, E.B.; NELTNER, A.E.; HOSMER, J.E. Articles of Reclaimed Polypropylene Compositions. WO2017003802A1, January 5, 2017. ⟨https://patents.google.com/patent/WO2017003802A1/en⟩ (accessed 2025-08-28).

[19] Trinseo Introduces Recycled Polystyrene for Direct Food Contact Applications | News | February 27, 2025 | *Trinseo*. ⟨https://www.trinseo.com/news-and-events/trinseo-news/2025/february/trinseo-introduces-recycled-polystyrene-for-direct-food-contact-applications⟩ (accessed 2025-08-28).

[20] Trinseo_rPS-Fast-Fact-Sheet-A4-Fast-Fact-Sheet-final.pdf. ⟨https://trinseo.widen.net/s/z5qmlrghqs/trinseo_rps-fast-fact-sheet-a4-fast-fact-sheet-final⟩ (accessed 2025-08-28).

[21] Trinseo and MagREEsource Collaborate to Advance Recycling of Products Containing Plastics and Magnetic Systems | News | *April 7, 2025* | *Trinseo*. ⟨https://www.trinseo.com/news-and-events/trinseo-news/2025/april/trinseo-and-magreesource-collaborate-to-advance-recycling-of-products-containing-plastics-and-magnetic-systems⟩ (accessed 2025-08-28).

[22] Trinseo Starts Up Polycarbonate Dissolution Pilot Facility in the Netherlands. ⟨https://investor.trinseo.com/home/news/news-details/2023/Trinseo-Starts-Up-Polycarbonate-Dissolution-Pilot-Facility-in-the-Netherlands/default.aspx⟩ (accessed 2025-08-28).

[23] D. Deshmukh, H. Kulkarni, D.S. Srivats, S. Bhanushali, A.P. More, Recycling of acrylonitrile butadiene styrene (ABS): a review, Polym. Bull. 81 (13) (2024) 1–38, https://doi.org/10.1007/s00289-024-05269-y.

[24] T. Lu, W.-T. Chen, Material recycling of acrylonitrile butadiene styrene (ABS) from toy waste using density separation and safer solvents, Resour. Conserv. Recycl 197 (2023) 107090, https://doi.org/10.1016/j.resconrec.2023.107090.

[25] A. Arostegui, M. Sarrionandia, J. Aurrekoetxea, I. Urrutibeascoa, Effect of dissolution-based recycling on the degradation and the mechanical properties of Acrylonitrile–Butadiene–Styrene copolymer, Polym. Degrad. Stab. 91 (11) (2006) 2768–2774, https://doi.org/10.1016/j.polymdegradstab.2006.03.019.

[26] L. Wang, Y. Liu, H. Lu, Z. Huang, Recycling of phosphorus-containing plastic based on the dual effects of switchable hydrophilicity solvents, Chemosphere 259 (2020) 127402, https://doi.org/10.1016/j.chemosphere.2020.127402.

[27] Y. Eom, H. Ju, Y. Park, D.W. Chae, Y.M. Jung, B.C. Kim, H.G. Chae, Effect of dissolution pathways of polyacrylonitrile on the solution homogeneity: thermodynamic- or kinetic-controlled dissolution, Polymer 205 (2020) 122697, https://doi.org/10.1016/j.polymer.2020.122697.

[28] B.A. Miller-Chou, J.L. Koenig, A review of polymer dissolution, Prog. Polym. Sci. 28 (8) (2003) 1223–1270, https://doi.org/10.1016/S0079-6700(03)00045-5.

[29] P.D. Krasicky, R.J. Groele, F. Rodriguez, Measuring and modelling the transition layer during the dissolution of glassy polymer films, J. Appl. Polym. Sci. 35 (3) (1988) 641–651, https://doi.org/10.1002/app.1988.070350307.

[30] E.E. Palchikova, I.S. Makarov, M.V. Mironova, M.I. Vinogradov, L.K. Golova, V. G. Kulichikhin, Phase transformations in a PAN–N-methylmorpholine-N-oxide–water system, Colloid J. 84 (6) (2022) 730–740, https://doi.org/10.1134/S1061933X22700120.

[31] J.S. Papanu, D.W. Hess, A.T. Bell, D.S. Soane, In situ ellipsometry to monitor swelling and dissolution of thin polymer films, J. Electrochem. Soc. 136 (4) (1989) 1195, https://doi.org/10.1149/1.2096852.

[32] Ş. Uğur, Ö. Pekcan, Determination of relaxation and diffusion activation energies during dissolution of latex film using *in Situ* fluorescence technique, Polymer 38 (22) (1997) 5579–5586, https://doi.org/10.1016/S0032-3861(97)00100-6.

[33] I. Devotta, V. Premnath, M.V. Badiger, P.R. Rajamohanan, S. Ganapathy, R. A. Mashelkar, On the dynamics of mobilization in swelling-dissolving polymeric systems, Macromolecules 27 (2) (1994) 532–539, https://doi.org/10.1021/ma00080a030.

[34] G. Melilli, S. Litwin, L. Vincent, N. Sbirrazzuoli, M.C.P. Roelands, J.C. van der Waal, R. Cuypers, N. Guigo, Monitoring *in-Situ* dissolution of Polystyrene-Acrylonitrile (SAN) via calorimetry and spectroscopy, J. Mol. Liq. 415 (2024) 126336, https://doi.org/10.1016/j.molliq.2024.126336.

[35] B. Narasimhan, N.A. Peppas, The physics of polymer dissolution: modeling approaches and experimental behavior. Polymer Analysis Polymer Physics; Advances in Polymer Science, Springer, Berlin, Heidelberg, 1997, pp. 157–207, https://doi.org/10.1007/3-540-61218-1_8.

[36] R.D. Arjanggi, J. Kansedo, Recent advancement and prospective of waste plastics as biodiesel additives: a review, J. Energy Inst. 93 (3) (2020) 934–952, https://doi.org/10.1016/j.joei.2019.08.005.

[37] A.P. Safronov, L.V. Adamova, Thermodynamics of dissolution of glassy polymers, Polymer 43 (9) (2002) 2653–2662, https://doi.org/10.1016/S0032-3861(02)00050-2.

[38] A.M. Basedow, K.H. Ebert, W. Feigenbutz, Polymer-solvent interactions: dextrans in water and DMSO, Makromol. Chem. 181 (5) (1980) 1071–1080, https://doi.org/10.1002/macp.1980.021810511.

[39] C.M. Hansen, Hansen Solubility Parameters: A User's Handbook, Second Edition, CRC Press, 2007.

[40] A. Benazzouz, L. Moity, C. Pierlot, M. Sergent, V. Molinier, J.-M. Aubry, Selection of a greener set of solvents evenly spread in the hansen space by space-filling design, Ind. Eng. Chem. Res. 52 (47) (2013) 16585–16597, https://doi.org/10.1021/ie402410w.

[41] S. Vyazovkin, A.K. Burnham, J.M. Criado, L.A. Pérez-Maqueda, C. Popescu, N. Sbirrazzuoli, ICTAC kinetics committee recommendations for performing kinetic computations on thermal analysis data, Thermochim. Acta 520 (1) (2011) 1–19, https://doi.org/10.1016/j.tca.2011.03.034.

[42] S. Vyazovkin, Isoconversional methodology, in: S. Vyazovkin (Ed.), In Isoconversional Kinetics of Thermally Stimulated Processes, Springer International Publishing, Cham, 2015, pp. 27–62, https://doi.org/10.1007/978-3-319-14175-6_2.

[43] N. Sbirrazzuoli, Is the Friedman method applicable to transformations with temperature dependent reaction heat? Macromol. Chem. Phys. 208 (14) (2007) 1592–1597, https://doi.org/10.1002/macp.200700100.

[44] S. Vyazovkin, Evaluation of activation energy of thermally stimulated solid-state reactions under arbitrary variation of temperature, J. Comput. Chem. 18 (3) (1997) 393–402, https://doi.org/10.1002/(SICI)1096-987X(199702)18:3<393::AID-JCC9>3.0.CO;2-P.

[45] S. Vyazovkin, Modification of the integral isoconversional method to account for variation in the activation energy, J. Comput. Chem. 22 (2) (2001) 178–183, https://doi.org/10.1002/1096-987X(20010130)22:2<178::AID-JCC5>3.0.CO;2-#.

[46] N. Sbirrazzuoli, Determination of pre-exponential factors and of the mathematical functions $f(\alpha)$ or $G(\alpha)$ that describe the reaction mechanism in a model-free way, Thermochim. Acta 564 (2013) 59–69, https://doi.org/10.1016/j.tca.2013.04.015.

[47] N. Sbirrazzuoli, Interpretation and physical meaning of kinetic parameters obtained from isoconversional kinetic analysis of polymers, Polymers 12 (6) (2020) 1280, https://doi.org/10.3390/polym12061280.

[48] N. Sbirrazzuoli, Advanced isoconversional kinetic analysis for the elucidation of complex reaction mechanisms: a new method for the identification of rate-limiting steps, Molecules 24 (9) (2019) 1683, https://doi.org/10.3390/molecules24091683.

[49] N. Sbirrazzuoli, Determination of pre-exponential factor and reaction mechanism in a model-free way, Thermochim. Acta 691 (2020) 178707, https://doi.org/10.1016/j.tca.2020.178707.

[50] S. Vyazovkin, N. Sbirrazzuoli, Isoconversional kinetic analysis of thermally stimulated processes in polymers, Macromol. Rapid Commun. 27 (18) (2006) 1515–1532, https://doi.org/10.1002/marc.200600404.

[51] N. Sbirrazzuoli, Kinetic analysis of complex chemical reactions by coupling model-free and model-fitting analysis, Thermochim. Acta 719 (2023) 179416, https://doi.org/10.1016/j.tca.2022.179416.

[52] CRC Handbook of Enthalpy Data of Polymer-Solvent Systems. Routledge & CRC Press. ⟨https://www.routledge.com/CRC-Handbook-of-Enthalpy-Data-of-Polymer-Solvent-Systems/Wohlfarth/p/book/9780367453831⟩ (accessed 2023-08-29).

[53] J.S. Papanu, D.W. Hess, D.S. Soane (Soong), A.T. Bell, Swelling of poly(Methyl Methacrylate) thin films in low molecular weight alcohols, J. Appl. Polym. Sci. 39 (4) (1990) 803–823, https://doi.org/10.1002/app.1990.070390404.

[54] S. Nur'aini, A. Zulfi, B.H. Arrosyid, A.F. Rafryanto, A. Noviyanto, D.A. Hapidin, D. Feriyanto, K.E. Saputro, K. Khairurrijal, N.T. Rochman, Waste Acrylonitrile Butadiene Styrene (ABS) incorporated with Polyvinylpyrrolidone (PVP) for potential water filtration membrane, RSC Adv. 12 (52) (2022) 33751–33760, https://doi.org/10.1039/d2ra05969j.

[55] R. Watanabe, A. Oishi, S. Nakamura, H. Hagihara, H. Shinzawa, Real-time monitoring of the thermooxidative degradation behavior of poly(Acrylonitrile-Butadiene-Styrene) using isothermal *in-Situ* Fourier transform infrared spectroscopy combined with principal component analysis, Polymer 283 (2023) 126243, https://doi.org/10.1016/j.polymer.2023.126243.

[56] N.L. Thomas, A.H. Windle, A theory of case II diffusion, Polymer 23 (4) (1982) 529–542, https://doi.org/10.1016/0032-3861(82)90093-3.

[57] L. Lapčík, L. Valko, Kinetic study of dissolution of poly(Vinyl Chloride) in Cyclohexanone, J. Polym. Sci. Part 2 Polym. Phys. 9 (4) (1971) 633–643, https://doi.org/10.1002/pol.1971.160090406.

[58] L. Lapčík, L. Valko, M. Mikula, V. Jančovičová, J. Panák, Kinetics of swollen surface layer formation in the diffusion process of polymer dissolution, in: K. Hummel, J. Schurz (Eds.), In Dispersed Systems, Steinkopff, Darmstadt, 1988, pp. 221–226, https://doi.org/10.1007/BFb0116788.

[59] K. Ueberreiter, F. Asmussen, Velocity of dissolution of polymers. Part I, J. Polym. Sci. 57 (165) (1962) 187–198, https://doi.org/10.1002/pol.1962.1205716515.

[60] J.S. Papanu, D.W. Hess, D.S. Soane, A.T. Bell, Dissolution of thin poly(Methyl Methacrylate) films in ketones, binary ketone/alcohol mixtures, and hydroxy ketones, J. Electrochem. Soc. 136 (10) (1989) 3077, https://doi.org/10.1149/1.2096404.

[61] S. Kovenklioglu, Experimental Investigation and Modeling of the Dissolution of Polymers and Filled Polymers, Polym. Eng. Sci. 38 (1) (1998) 90–100, https://doi.org/10.1002/pen.10168.

[62] J.S. Papanu, D.S. Soane (Soong), A.T. Bell, D.W. Hess, Transport models for swelling and dissolution of thin polymer films, J. Appl. Polym. Sci. 38 (5) (1989) 859–885, https://doi.org/10.1002/app.1989.070380509.

[63] H.L. Frisch, Sorption and transport in glassy polymers–a review, Polym. Eng. Sci. 20 (1) (1980) 2–13, https://doi.org/10.1002/pen.760200103.
[64] L. Yilmaz, İ. Tosun, T. Gürkan, Ü. Gülçat, Anomalous diffusion of liquids in glassy polymers, Math. Model 4 (6) (1983) 535–543, https://doi.org/10.1016/0270-0255(83)90013-1.
[65] M. Jamali Moghadam Siahkali, N. Guigo, N. Sbirrazzuoli, Cross-linking mechanisms of a rigid plant oil-based thermoset from furfural-derived cyclobutane, Macromolecules 56 (2) (2023) 404–415, https://doi.org/10.1021/acs.macromol.2c02219.
[66] N.L. Thomas, A.H. Windle, A deformation model for Case II diffusion, Polymer 21 (6) (1980) 613–619, https://doi.org/10.1016/0032-3861(80)90316-X.
[67] C. Du, R.J. Hill, Linear viscoelasticity of weakly cross-linked hydrogels, J. Rheol. 63 (1) (2019) 109–124, https://doi.org/10.1122/1.5052160.